

# High harmonics from backscattering of delocalized electrons

Chuan Yu, Ulf Saalmann, and Jan M. Rost

Max-Planck-Institut für Physik komplexer Systeme, Nöthnitzer Str. 38, 01187 Dresden, Germany

(Dated: February 23, 2021)

Electron backscattering is introduced as mechanism to enhance high-harmonic generation in solid-state like systems with broken translational symmetry. As a paradigmatic example we derive for a finite chain of  $N$  atoms the harmonic cut-off through backscattering of electrons in the conduction band from the edges of the chain. We also demonstrate a maximum in the yield of the high harmonics from the conduction band if twice the quiver amplitude of the driven electrons equals the length of the chain. High-harmonic spectra as a function of photon energy are shown to be equivalent if the ratio of chain length to the wavelength of the light is kept constant. Our quantum results are corroborated by a (semi-)classical trajectory model with refined spatial properties required to describe dynamics with trajectories in the presence of broken translational symmetry.

Since the pioneering experiment by Ghimire et al. [1] high-harmonic generation (HHG) with strong laser fields applied to solids has been a focus of experimental and theoretical research with first reviews available [2–4]. The so-called “three-step model” [5] is key to understand the microscopic electron dynamics of HHG in atoms and molecules semi-classically in terms of classical trajectories [6]. It has been adapted successfully for interband HHG in solids [7–9], suggesting that fundamental properties of high harmonics are ruled by the same basic principles from atoms to the solid state. On the other hand, a solid-state environment should offer more possibilities to influence these phenomena than an atom due to the larger structural complexity and variability [10–14]. Indeed, under suitable conditions, a solid-state HHG spectrum exhibits several cut-offs [10, 15] due to the (band-)structured continuum of solid-state electrons, in contrast to the single atomic cut-off.

In an atomic context, cut-offs can be extended if the laser-driven electron acquires a larger momentum through backscattering from another atom or ion. This requires a large distance of the order of the atomic quiver amplitude  $A_0/\omega_0$  between the back-scattering and recombining ion, where  $A_0$  is the peak vector potential and  $\omega_0$  the carrier frequency of the laser. This can theoretically be achieved in laser-assisted ion-atom collisions with a suitable impact parameter [16] or for above-threshold ionization in rare-gas clusters with a suitable size, as demonstrated recently in an experiment [17], but not in molecules which are typically too small. Solid-state like systems, on the other hand, can easily match the spatial requirements set by the quiver amplitude of conduction-band electrons and any irregularity in their periodicity may give rise to backscattering. Indeed, we will analytically predict and numerically demonstrate in the following significantly extended HHG cut-offs through backscattering of delocalized electrons.

To keep the situation as simple as possible we investigate HHG from a chain of  $N$  atoms with a lattice constant (interatomic distance) of  $d = 7$  a.u. and 4 active electrons per atom as introduced before [18]. We will show that extended cut-offs through backscattering from the edge can occur and that HHG is most efficient if the full excursion

of the excited laser-driven electron (twice the quiver amplitude  $x_q$ ) matches the length of the chain, i. e., if  $N \approx N_q$  with the latter defined by  $2x_q \equiv N_q d$ . Motivated by simple scaling arguments and the (semi-)classical trajectory picture for interband harmonics, the predicted cut-off and maximal high-harmonic yield is accurately reflected in the HHG spectra obtained with the laser-driven flux of the  $4N$  electrons. Apart from small modifications we find the electron dynamics in a chain with  $N \gtrsim 10$  well described with the band structure of the periodic system.

For the chain of  $N$  atoms we compute the harmonic spectrum generated per atom

$$S_N(\omega) \propto N^{-2} \left| \int dt J_{\text{tot}}(t) W(t) e^{-i\omega t} \right|^2, \quad (1)$$

where  $J_{\text{tot}}(t)$  is the total current in the system and  $W(t)$  is a window function of the laser-pulse-envelope shape for improving the signal-to-noise ratio. Details of the methods and parameters used as well as the periodic treatment for the limit  $N \rightarrow \infty$  can be found in [19]. The laser pulse with frequency  $\omega_0$  is linearly polarized along the chain and described in dipole approximation by the vector potential  $A(t) = A_0 \sin^2(\omega_0 t / [2n_{\text{cyc}}]) \sin(\omega_0 t)$  for  $0 \leq t \leq 2\pi n_{\text{cyc}} / \omega_0$  and  $A(t) = 0$  otherwise. All results are obtained with  $n_{\text{cyc}} = 9$  and  $A_0 = 0.21$ , but backscattering is not restricted to specific laser parameters as will become clear. Atomic units (a.u.) are used throughout unless stated otherwise.

An overview of the results is presented in Fig. 1 for the three laser wavelengths  $\lambda = 1600, 2400$  and  $3200$  nm. The vertical structure in panels a–c for large  $N$  signals that the HHG spectra approach the periodic limit  $N \rightarrow \infty$ . However, in the lower central part of Figs. 1a–c one sees a stronger HHG response which prevails for a certain range of systems sizes. To see this more clearly, Figs. 1d–f show (in red) spectra at the system sizes  $N = 16, 24$  and  $32$ , where the HHG response for midsize harmonic orders is enhanced. These selected system sizes (marked by horizontal dashed lines in Figs. 1a–c) have the widest enhancement region. The enhancement is particularly evident in comparison to the periodic limit (grey areas). The latter is apparently reached in

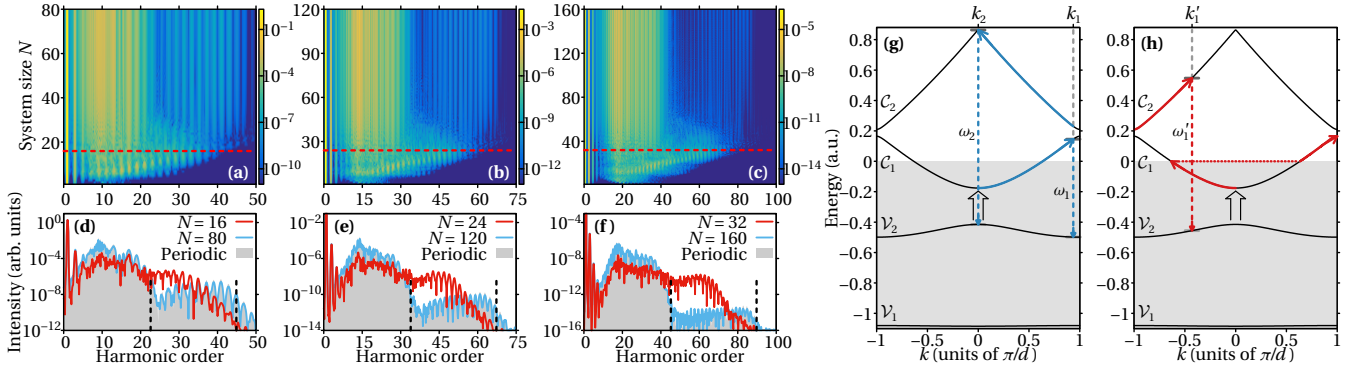


FIG. 1. HHG spectra as a function of harmonic order and system size  $N$  for wavelengths of 1600 nm (a), 2400 nm (b) and 3200 nm (c) and for the same wavelengths but at fixed  $N = 16$  (d),  $N = 24$  (e), and  $N = 32$  (f), indicated by horizontal dashed lines in (a-c). The spectra of the periodic system are shown as shaded area for comparison. The dashed lines indicate the estimates of the 1st and 2nd cut-off for the periodic system at  $\omega_1$  and  $\omega_2$ , specified in the text. (g) Sketch of the  $k$ -space dynamics in the periodic system, for an electron excited to the bottom of the  $C_1$ -band at  $A(t_0) \approx -A_0$ . The maximal  $C_1$ - $\mathcal{V}_2$  and  $C_2$ - $\mathcal{V}_2$  band energy differences (i.e., the cut-offs  $\omega_1$  and  $\omega_2$ ) are achieved at  $k_1 = 2A_0$  and  $k_2 = 0$ . (h) Sketch of the  $k$ -space dynamics in the finite system, with an edge backscattering event in the  $C_1$ -band at the vacuum level occurring at  $A(t_s) = -A_0$ . The horizontal dotted line represents the sign change of  $k(t)$  due to backscattering. With a subsequent band-gap transition to the  $C_2$ -band, this sketch corresponds to the maximally achievable harmonic frequency in the backscattering case  $\omega'_1$  at  $k'_1$  (see text).

the longest chains considered for each wavelength ( $N = 80, 120$  and  $160$ , respectively), which are presented in blue.

The periodic spectra exhibit two clear steps corresponding to the end (cut-off) of a 1st and 2nd plateau marked by dashed vertical lines. As one can see from the band structures in Fig. 1g, these cut-offs represent the maximally possible recombination energies [15] with the valence band  $\mathcal{V}_2(k)$ :  $\omega_1 = C_1(k_1) - \mathcal{V}_2(k_1) = 0.64$  at  $k_1 = 2A_0 = 0.94 \pi/d$  and  $\omega_2 = C_2(k_2) - \mathcal{V}_2(k_2) = 1.28$  at  $k_2 = 0$ . Due to the band structure, the lowest valence band  $\mathcal{V}_1$  does not actively participate in the HHG processes. An electron, excited from the 2nd valence band  $\mathcal{V}_2$  at  $t_0$ , preferentially enters the 1st conduction band  $C_1$  at  $k_0 \approx 0$  near the  $\Gamma$ -point ( $k = 0$ ) and subsequently moves with momentum

$$k(t) = A(t) - A(t_0) + k_0. \quad (2)$$

This time-dependent  $k$ -space motion always holds in the periodic limit, but can be modified by backscattering in finite systems, as will be discussed below.

The enhanced spectra (red in Fig. 1d-f) exhibit a small dip at the 1st cut-off but the enhancement does not extend to the 2nd cut-off. This observation suggests that the enhancement is not due to a more efficient mechanism to enter  $C_2$  preserving the original  $k(t)$ . Rather, it must be a process which changes  $k(t)$ . This can be achieved by elastic scattering in the presence of a laser field. Indeed, as we will see, the enhancement is due to electrons in  $C_1$ , being backscattered from the edge of the chain.

When an electron wavepacket approaches the system edge, it can either be reflected from it (i.e., being backscattered) or leak out of the system (i.e., being ionized). Backscattering (ionization) will be dominant if its mean energy is lower (higher) than the vacuum level. In the classical three-step description, backscattering at a time  $t_s$  is

assumed to be elastic, resulting in a sign change of the instantaneous momentum

$$k(t > t_s) = A(t) - 2A(t_s) + A(t_0) - k_0. \quad (3)$$

In a solid-state system the electron (and the accompanying hole) suffer the momentum kick while moving on their respective band with dispersion  $E(k)$ . This is illustrated in Fig. 1h for the electron. In general, the band energy at backscattering must be below the vacuum level  $E = 0$  to avoid ionization. Therefore, the maximal momentum at backscattering is  $k_s = 0.285$ , defined by  $C_1(k_s) = 0$ . Since the electron can acquire at most a momentum of  $2A_0$  through (unperturbed) interaction with the laser field, the maximal final momentum is  $k'_1 = k_s + 2A_0 - 2\pi/d$  in the first Brillouin zone (BZ) leading to the recombination energy  $\omega'_1 = C_2(k'_1) - \mathcal{V}_2(k'_1) = 1.0$  which defines the 1st cut-off energy *extended through backscattering*. Indeed, this corresponds to harmonic order 35, 53, 70 for the wavelengths  $\lambda = 1600, 2400, 3200$  nm, respectively, where the yield of the enhanced spectra (red) in Figs. 1d-f decreases.

In passing we note, that without backscattering, the electron in Fig. 1h would never have the chance to pass the BZ boundary and enter the  $C_2$ -band via a subsequent band-gap transition. Hence, edge backscattering suggests itself as a pathway to high-energy states in analogy to backscattered electrons from an ion in the atomic context. There, however, backscattering only leads to higher photo-electron energies [17, 20], but not to larger cut-offs in HHG. This is mainly due to the fact that the electron's wavefunction in the atomic context is usually spatially localized on the ion (playing the role of the hole) and the continuum electron wavepacket. The lacking overlap prevents recombination necessary for HHG between the energetic electron far away

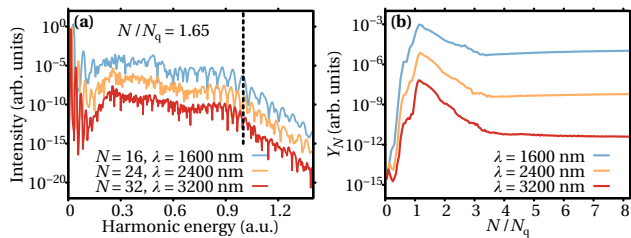


FIG. 2. The HHG spectra from Fig. 1d–f as function of photon energy (a) and their integrated yield  $Y_N$  beyond the 1st cut-off  $\omega_1$  as a function of scaled system size  $N/N_q$  (b). The vertical dashed line in panel (a) represents the edge-backscattering cut-off at  $\omega'_1 = 1.0$ , discussed in the text.

from the ion available for recombination. In solid-state like systems, on the other hand, we deal with spatially delocalized Bloch electrons, for which overlap of electron-hole wavefunctions can be more easily achieved [21]. Moreover, electrons reflected by the edges of an extended system continue to move inside the system, allowing them to recombine with significant wavefunction overlap. Therefore, backscattering represents a promising mechanism for increasing the energy of solid-state harmonics.

As a next step we work out which role the spatial extension of the chain plays for backscattering. To this end we vary in Fig. 2 the wavelength of the light while keeping the vector potential fixed. The latter ensures that the dynamics in momentum space, and in particular the energy gain through backscattering depending on  $A_0$  as discussed so far, remains the same while through the variation of the wavelength the quiver amplitude  $x_q \propto A_0 \lambda$  changes linearly, resulting in different scales for the spatial dynamics. Hence, locking the ratio of chain length versus wavelength  $N/\lambda$  in addition to an identical  $A_0$  should provide similar conditions for the high-harmonics-generating electron dynamics and we expect similar spectra, provided the harmonic yield is not shown as a function of the harmonic order but of the harmonic energy instead, as done in Fig. 2a. The similarity of the three spectra with the extended cut-off at  $\omega'_1 = 1.0$  is evident.

In Fig. 2b we demonstrate that this similarity implies a universal ratio  $N_q/\lambda$  where the largest enhancement of the high harmonic yield for edge backscattering occurs. For this purpose we integrate the harmonic yield in the spectral region of enhancement,  $Y_N = \int_{\omega_1} d\omega S_N(\omega)$ . That the curves level off for large  $N$  simply reflects convergence to the periodic limit without edge backscattering. That all three integrated yields have a similar shape over the entire scaled range of  $N$  illustrates the universality of the underlying strong-field dynamics of delocalized electrons provided that momentum and spatial dynamics is equivalent. Most interesting in the context of backscattering is the sharp rise and maximum of  $Y_N$  which occurs close to  $N/N_q = 1$  for different wavelengths with the critical number of atoms  $N_q = 2x_q/d$ , where the length  $N_q d$  of the chain equals the full quiver

excursion  $2x_q$  of the excited electron.

We note that while the momentum scale  $A_0$ , the vector potential, is a property of the light only, this is not the case for the spatial scale  $x_q$ , the quiver amplitude, which depends also on the band structure. With the instantaneous momentum given by Eq. (2), the position-space motion of a Bloch electron in band  $\mathcal{B}$  reads

$$\Delta x_{\mathcal{B}}(t) \equiv x_{\mathcal{B}}(t) - x_{\mathcal{B}}(t_0) = \int_{t_0}^t dt' \frac{d}{dk} \mathcal{B}(k) \Big|_{k=k(t')}. \quad (4)$$

Within the Kane band approximation [22, 23], an explicit expression for  $x_q$  can be given which is even analytically solvable if the electron moves with initial condition  $A(t_0) = 0$  in the conduction band. In this case  $x_q = [A_0/(m_* \omega_0)] \arctan(a)/a$ , with  $a = A_0/k_*$ , where  $m_*$  is the effective mass of the electron and  $k_*$  the band's momentum scale [23].

Finally, we discuss how the HHG time-frequency profile (shown in Fig. 3) obtained by Gabor transforming the quantum current in Eq. (1), can be mapped onto classical trajectories from Eq. (4) for the electron-hole pair. This is for at least two reasons not straightforward. (i) Even in the periodic-system case, the semi-classical three-step trajectory picture with more than one conduction band has only been demonstrated successfully for situations where the maximal electron momentum exceeds the BZ boundary ( $2A_0 > \pi/d$ ) and therefore takes the excited electron across the gap between  $\mathcal{C}_1$  and  $\mathcal{C}_2$  and eventually gaps between higher bands [15]. (ii) It is unclear if the backscattering mechanism can be described adequately with trajectories. Hence, the more intricate circumstances of backscattering provide also a chance to refine the semi-classical trajectory model for HHG, which is, however, beyond the scope of the present work. Here, we only sketch the feasibility of such

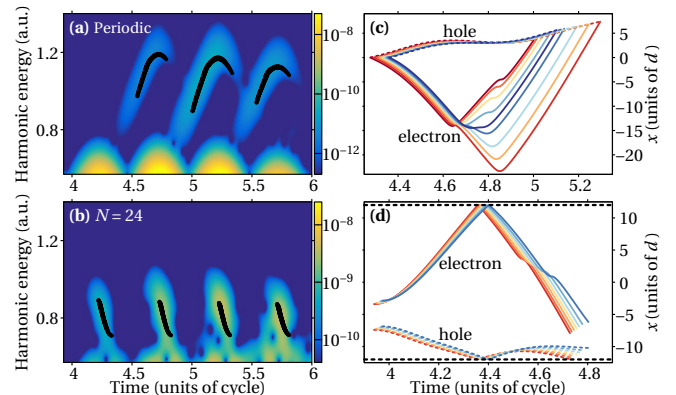


FIG. 3. HHG time-frequency profile at  $\lambda = 2400$  nm for the periodic system (a) and a finite chain of  $N = 24$  (b), respectively. The black dots are traces obtained from the semi-classical electron-hole recollision model, without (a) and with (b) backscattering. (c) and (d) provide representative trajectories forming the traces in (a) and (b) in real space. In the backscattering case, an electron-hole separation of  $\delta L = 4d$  is chosen as initial condition. The dashed lines in (d) indicate the system edges taken as  $\pm Nd/2$ .

an enterprise.

Regarding the periodic case (i) we relax the (standard) condition of tunneling at the  $\Gamma$ -point ( $k_0=0$ ) and allow a small interval  $|k_0| \leq 0.18\pi/d$  about  $k_0=0$  as initial condition for the trajectory of the tunneled electron on  $\mathcal{C}_1$ . Doing so, the black HHG traces in the time-frequency plane result for the 2nd HHG plateau (Fig. 3a) with the corresponding electron-hole trajectories shown in Fig. 3c. As the electron is much lighter than the hole (manifest in the smaller energy dispersion of  $\mathcal{V}_2$  compared to  $\mathcal{C}_1$  in Fig. 1g), its excursion on the way to recombination is larger than the one of the hole. Moreover, electron and hole move initially into different directions as their respective band dispersions have opposite sign. As one can see in Fig. 3c for different electron and hole trajectories starting at the position zero, respectively, the standard semi-classical condition  $\Delta x_C(t_r) - \Delta x_V(t_r) = 0$  for recombination is fulfilled at different times  $t_r$  with high harmonic emission energy  $\mathcal{C}_2(k) - \mathcal{V}_2(k)$  linked to time through the dependence  $k = k(t)$ .

Note, that starting the trajectories at  $x = 0$  with zero separation is just a convention, probably inherited from HHG in atoms, where the position of the ion (taken at zero) indeed fixes the entire recombination dynamics to  $x = 0$ . In the solid-state context with delocalized electrons, however, the electron and associated hole trajectories can be born and recombine with an arbitrary separation  $\delta L = \Delta_{C_V}(t_0) = \Delta_{C_V}(t_r)$  with  $\Delta_{C_V}(t) \equiv x_C(t) - x_V(t)$  and centered about another location but  $x = 0$ , which is just another way to fulfill the standard semi-classical recombination condition [2, 7, 8]

$$\Delta x_C(t_r) - \Delta x_V(t_r) = \Delta_{C_V}(t_r) - \Delta_{C_V}(t_0) = 0 \quad (5)$$

and lead to the same traces in Fig. 3a. Furthermore, trajectories can turn around due to the dependence of  $k(t)$  on the vector potential  $A(t)$  akin to continuum electron trajectories in an atomic situation, but also due to sign changes in the dispersion  $d\mathcal{B}/dk$  of the energy bands, a feature not present in atoms.

We turn now to the situation of backscattering (ii), illustrated with a chain of  $N = 24$  in Figs. 3b, d. As one sees right away, the time-frequency traces differ drastically from the periodic situation. We can describe the traces with classical trajectories modified in two aspects compared to the standard scenario in Fig. 3c. Firstly, if the energy of the electron is below the vacuum level,  $\mathcal{C}_1(t_s) < 0$ , backscattering takes place by elastic reflection of the trajectories at the chain edges (shown dashed in Fig. 3d). This means that for  $t > t_s$  Eq. (3) holds instead of (2). Secondly, the electron and the associated hole trajectory are born and recombine with a spatial separation  $\delta L$  centered about a specific location in the chain which is no longer arbitrary but necessary to give the traces in Fig. 3b in agreement with the quantum time-frequency profile. The spatial separation  $\delta L$  implies that not the entire length of the chain is

available for the high-harmonics-generating quiver dynamics of electron and hole trajectories. This is consistent with the fact that the integrated high-harmonic yield  $Y_N$  peaks systematically for values of  $N/N_q$  slightly larger than one in Fig. 2b. At the present level of a simple classical trajectory description, the spatial separation  $\delta L$  is a parameter whose value emerges through comparison with the (quantum) time-frequency pattern of HHG. In the classical limit  $\lambda \rightarrow \infty$ , we expect this parameter to become irrelevant as its scaled value  $\delta L/\lambda$  tends to zero. Indeed, careful inspection of Fig. 2b reveals that the offset from  $N/N_q = 1$  becomes smaller for larger  $\lambda$ .

To summarize, we have established electron backscattering as a mechanism to extend the cut-off for solid-state like harmonics in systems with an inherent length scale due to broken translational symmetry. For simplicity and consistency, we have chosen to demonstrate and analyze backscattering with finite chains of atoms solving the many-electron dynamics based on density functional theory. This has allowed us to link the quiver amplitude of the driven electron to the extension of the system, revealing that one achieves the highest integrated harmonic yield beyond the 1st cut-off of the periodic system, if twice the quiver amplitude is approximately equal to the length of the atomic chain. The band energy at the momentum where backscattering takes place must be below the vacuum level of the system, otherwise ionization dominates reflection. This is a universal condition for the extended cut-off, which takes, however different values depending on the band structure.

Akin to the time-frequency profile of standard interband high harmonics, also harmonics due to backscattering can be described in terms of a simple trajectory picture with elastic reflection from the edges of the atomic chain and a finite distance of electron and hole trajectories at birth and recombination. Since spatial properties become relevant for systems with broken translational symmetry, they will be interesting and helpful to refine semi-classical trajectory descriptions.

Backscattering as introduced here has close analogies in extended atomic systems. However, in the latter it leads only to higher energies in laser-driven photo-ionization (often termed above-threshold ionization), but not to larger high-harmonic cut-offs, since the localized electrons in atomic systems lack the ability for overlap of electron amplitudes at large distances which is possible for the delocalized electrons in solid-state like systems. Other sources of breaking the periodicity of the solid-state system, such as impurities, domain walls or grain boundaries, may also induce backscattering and ensuing effects on HHG. Work in this direction is underway.

CY acknowledges discussion with Lars Bojer Madsen in the early stage of this work.

- 
- [1] S. Ghimire, A. D. DiChiara, E. Sistrunk, P. Agostini, L. F. DiMauro, and D. A. Reis, *Observation of high-order harmonic generation in a bulk crystal*. *Nature Phys.* **7**, 138 (2011).
- [2] G. Vampa and T. Brabec, *Merge of high harmonic generation from gases and solids and its implications for attosecond science*. *J. Phys. B* **50**, 083001 (2017).
- [3] S. Ghimire and D. A. Reis, *High-harmonic generation from solids*. *Nature Phys.* **15**, 10 (2019).
- [4] C. Yu, S. Jiang, and R. Lu, *High-order harmonic generation in solids: A review on recent numerical methods*. *Adv. Phys. X* **4**, 1562982 (2019).
- [5] M. Lewenstein, P. Balcou, M. Y. Ivanov, A. L'Huillier, and P. B. Corkum, *Theory of high-harmonic generation by low-frequency laser fields*. *Phys. Rev. A* **49**, 2117 (1994).
- [6] G. van de Sand and J. M. Rost, *Irregular orbits generate higher harmonics*. *Phys. Rev. Lett.* **83**, 524 (1999).
- [7] G. Vampa, C. R. McDonald, G. Orlando, D. D. Klug, P. B. Corkum, and T. Brabec, *Theoretical analysis of high-harmonic generation in solids*. *Phys. Rev. Lett.* **113**, 073901 (2014).
- [8] G. Vampa, C. R. McDonald, G. Orlando, P. B. Corkum, and T. Brabec, *Semiclassical analysis of high harmonic generation in bulk crystals*. *Phys. Rev. B* **91**, 064302 (2015).
- [9] A. M. Parks, G. Ernotte, A. Thorpe, C. R. McDonald, P. B. Corkum, M. Taucer, and T. Brabec, *Wannier quasi-classical approach to high harmonic generation in semiconductors*. *Optica* **7**, 1764 (2020).
- [10] G. Ndabashimiye, S. Ghimire, M. Wu, D. A. Browne, K. J. Schafer, M. B. Gaarde, and D. A. Reis, *Solid-state harmonics beyond the atomic limit*. *Nature* **534**, 520 (2016).
- [11] N. Tancogne-Dejean, O. D. Mücke, F. X. Kärtner, and A. Rubio, *Impact of the electronic band structure in high-harmonic generation spectra of solids*. *Phys. Rev. Lett.* **118**, 087403 (2017).
- [12] D. Bauer and K. K. Hansen, *High-harmonic generation in solids with and without topological edge states*. *Phys. Rev. Lett.* **120**, 177401 (2018).
- [13] T. T. Luu and H. J. Wörner, *Measurement of the Berry curvature of solids using high-harmonic spectroscopy*. *Nat. Commun.* **9**, 916 (2018).
- [14] R. E. F. Silva, Á. Jiménez-Galán, B. Amorim, O. Smirnova, and M. Ivanov, *Topological strong-field physics on sub-laser-cycle timescale*. *Nat. Photonics* **13**, 849 (2019).
- [15] T. Ikemachi, Y. Shinohara, T. Sato, J. Yumoto, M. Kuwata-Gonokami, and K. L. Ishikawa, *Trajectory analysis of high-order-harmonic generation from periodic crystals*. *Phys. Rev. A* **95**, 043416 (2017).
- [16] M. Lein and J. M. Rost, *Ultra-high harmonics from laser-assisted ion-atom collisions*. *Phys. Rev. Lett.* **91**, 243901 (2003).
- [17] Z. Wang, A. Camacho Garibay, H. Park, U. Saalman, P. Agostini, J. M. Rost, and L. F. DiMauro, *Universal high-energy photoelectron emission from nanoclusters beyond the atomic limit*. *Phys. Rev. Lett.* **124**, 173201 (2020).
- [18] K. K. Hansen, T. Deffge, and D. Bauer, *High-order harmonic generation in solid slabs beyond the single-active-electron approximation*. *Phys. Rev. A* **96**, 053418 (2017).
- [19] C. Yu, H. Irvani, and L. B. Madsen, *Crystal-momentum-resolved contributions to multiple plateaus of high-order harmonic generation from band-gap materials*. *Phys. Rev. A* **102**, 033105 (2020).
- [20] G. G. Paulus, W. Becker, W. Nicklich, and H. Walther, *Rescattering effects in above-threshold ionization: a classical model*. *J. Phys. B* **27**, L703 (1994).
- [21] L. Yue and M. B. Gaarde, *Imperfect recollisions in high-harmonic generation in solids*. *Phys. Rev. Lett.* **124**, 153204 (2020).
- [22] E. O. Kane, *Band structure of indium antimonide*. *J. Phys. Chem. Solids* **1**, 249 (1957).
- [23] See supplemental material at [url]; For the present parameters  $m_* = 0.167$  and  $k_* = 0.2$  leading to  $x_q = 4.62A_0/\omega_0$  and  $N_q = \lambda/165$  nm.